Nucleic Acids Research, 2025, **53**, gkaf157
https://doi.org/10.1093/nar/gkaf157
Genome integrity, repair and replication

MutLγ enforces meiotic crossovers in *Arabidopsis thaliana*

Stéphanie Durand, Qichao Lian, Victor Solier, Joiselle Blanche Fernandes, Raphael Mercier *

Department of Chromosome Biology, Max Planck Institute for Plant Breeding Research, Carl-von-Linné-Weg 10, 50829 Cologne, Germany
*To whom correspondence should be addressed. Email: mercier@mpipz.mpg.de

Abstract

During meiosis, each chromosome pair experiences at least one crossover (CO), which directs their balanced segregation in addition to shuffling genetic information. COs tend to be away from each other, a phenomenon known as CO interference. The main biochemical pathway for CO formation, which is conserved in distant eukaryotes, involves the ZMM proteins together with the MLH1–MLH3 complex (MutLγ). Here, we aim to clarify the role of MutLγ in CO formation in *Arabidopsis thaliana*. We show that AtMutLγ is partially dispensable for ZMM-dependent CO formation. HEI10 large foci—that mark CO sites in wild-type—form at a normal level in *mlh1* and *mlh3* mutants, but are inefficiently matured into COs. Mutating the *MUS81* nuclease in either *mlh1* or *mlh3* leads to chromosome fragmentation, which is suppressed by further mutating the *zmm msh5*. This suggests that in the absence of MutLγ, recombination intermediates produced by ZMMs are resolved by MUS81, which does not ensure CO formation. Finally, CO interference is marginally affected in *mlh1*, which is compatible with a random sub-sampling of normally patterned CO sites. We conclude that AtMutLγ imposes designated recombination intermediates to be resolved exclusively as COs, supporting the view that MutLγ asymmetrically resolves double-Holliday junctions, yielding COs.

Graphical abstract

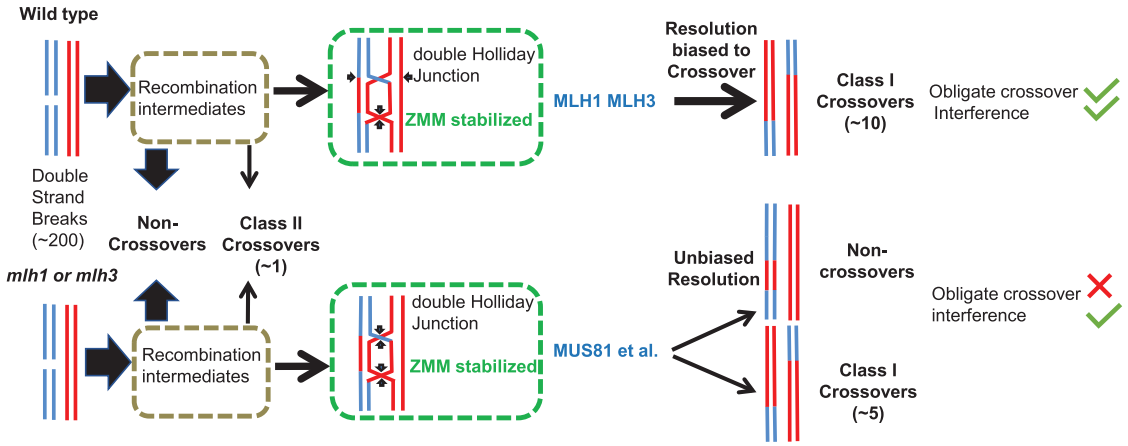

Introduction

Meiotic recombination initiates with the formation of a large number of DNA double-strand breaks followed by strand exchange with the homologous chromosomes forming DNA joint-molecule intermediates. A subset of these joint molecules is matured into double Holliday junctions (dHJs), two adjacent branched DNA structures that contain four double-stranded arms [1–3]. The formation of dHJs is promoted by a group of evolutionarily conserved proteins collectively named ZMMs (originally for the yeast Zip1-4, Msh4-5, and Mer3) [4]. Holliday junctions are symmetrical and their resolution can in principle lead to both crossovers (COs) and non-crossovers (NCOs), but, at least in budding yeast, they are processed asymmetrically by the MLH1/MLH3 (MutLγ) complex, yielding almost exclusively COs [5–10]. Consistently, mutation of either MLH1 or MLH3 reduces meiotic CO formation in yeast and mice, provoking spore unviability and sterility. Purified yeast Mlh1–Mlh3 has endonuclease activity *in vitro*, which is required for its pro-CO function *in vivo* [7, 8, 11–19]. Further in *vitro* studies with mammalian proteins confirmed the capacity of MutLγ to cleave DNA, an activity promoted by EXO1 and Proliferating-Cell-Nuclear-Antigen (PCNA), and suggested a mechanism for the biased processing of dHJs into COs [17, 18, 20, 21]. The COs promoted by the ZMMs and MutLγ, are called class I COs, and their locations on meiotic chromosomes are marked by prominent MLH1 foci at the end of pachytene [22, 23]. A second minor pathway is independent of ZMMs

Received: September 23, 2024. **Revised:** February 7, 2025. **Editorial Decision:** February 13, 2025. **Accepted:** March 11, 2025
© The Author(s) 2025. Published by Oxford University Press on behalf of Nucleic Acids Research.
This is an Open Access article distributed under the terms of the Creative Commons Attribution-NonCommercial License (https://creativecommons.org/licenses/by-nc/4.0/), which permits non-commercial re-use, distribution, and reproduction in any medium, provided the original work is properly cited. For commercial re-use, please contact reprints@oup.com for reprints and translation rights for reprints. All other permissions can be obtained through our RightsLink service via the Permissions link on the article page on our site—for further information please contact journals.permissions@oup.com.

and involves structure-specific DNA endonuclease including MUS81 [24].

In *Arabidopsis*, the ZMM proteins are responsible for most COs, with a ∼90% drop in CO formation in the absence of any of them [25, 26]. Like in mammals, MLH1 and MLH3 proteins accumulate in bright foci at future class I CO sites at late pachytene and persist until diakinesis [27–29]. Accordingly, MLH1 foci are absent at diakinesis in the *zmm* mutants *hei10* (*Zip3* homolog) and *zip4* [27, 30]. Disruption of *MLH3* leads to the loss of about half of the meiotic crossovers, a milder defect than a *zmm* mutant, associated with the loss of the obligate crossover and the presence of univalents [28]. *Arabidopsis* mutants in *MLH1* have fertility defects, but to our knowledge, their meiotic phenotype was not described [31]. Here we aimed to clarify the function of MutLγ in *Arabidopsis* meiosis, and we conclude that the function of AtMutLγ is to impose ZMM recombination intermediates to be resolved exclusively as COs, which is compatible with the proposed biochemical function in processing dHJs asymmetrically.

Materials and methods

Plant materials and growth conditions

Arabidopsis thaliana plants were cultivated in growth chambers or greenhouses (21°C in 16 h day, 18°C in 8 h night, 60% humidity). Wild-type Col-0 and L*er*-1 are 186AV1B4 and 213AV1B1 from the Versailles *A. thaliana* stock center (http://publiclines.versailles.inra.fr/). The mutant alleles used in this study are: *mlh1-2* (Col, N1008089, SK25975, K#123), *mlh3-3* (Col, N619674, SALK_119 674, K#309), *mus81-2* (Col, N607515, SALK_107 515, K#133) [32], *msh5-3* (Col, N841758, SAIL_1056_F12, K#124), *HEI10*^{OE} (Col, *C2 line,* pGreen0029-HEI10Col-H2, K#244) [33], *hei10-2* (Col, N514624, SALK_014 624, K#010) [30], and *mlh1-3* (L*er*, K#344) (Supplementary Fig. S1).

To generate double mutant *mlh1-2* HEI10^{oe} in Col background, homozygotes HEI10^{oe} (*C2*) were crossed as female with heterozygotes *mlh1-2*± as male. As the *MLH1* gene and the *HEI10* insertion are linked on chromosome 4, an F2 plant homozygous for the *HEI10* insertion and *mlh1*± was selfed, and double homozygous plants were selected in the resulting F3 population. Those double *mlh1-2* HEI10^{oe} were used for MLH1/HEI10 foci counting. The *mlh1-3* mutant allele in the L*er* background was obtained by CRISPR technology using two guides GATGATTACGGGAAAATCG and CCTGTGACTCCTCTGGTTG [34]. Transformations were performed with floral dipping. Plant transformants (T1) were selected by seed fluorescence. T2 seeds without fluorescence were selected and screened for mutations by polymerase chain reaction (PCR) and Sanger sequencing of the targeted locus.

To generate *mlh1-2*/*mlh1-3* in Col/L*er* and the wild-type control Col/L*er*, heterozygotes *mlh1-2*± were crossed as female with heterozygotes *mlh1-3*± as male. The *mlh1*−/− plants and their wild-type sister were used for HEI10 foci counting, bivalent analysis, and fertility analysis and were reciprocally backcrossed with wild-type Col to generate the BC1 populations to be sequenced (see below).

To generate *HEI10*± in Col/L*er*, *hei10-2*± Col were crossed as female with wild-type L*er* as male. Sister plants *HEI10*± and wild type were used for MLH1/HEI10 co-foci counting, bivalent analysis, and fertility measurements and were reciprocally backcrossed with wild-type Col to generate the BC1 (back-cross 1) populations to be sequenced.

Fertility

The fertility analysis of *Arabidopsis* plants was measured by counting the number of seeds per silique. At least 10 siliques sampled on the primary stem were analyzed per plant. Sister wild-type and mutant plants from segregating populations grown in the same environment were compared. The siliques were incubated in 70% ethanol. Once the siliques were transparent, they were imaged on a regular scanner. Seeds were counted manually using the ZEN Software (Carl Zeiss Microscopy).

Cytology

Chromosome 4′,6-Diamidin-2-phenylindol (DAPI) spreads [35] : Young inflorescences were harvested from *Arabidopsis* plants and fixed in freshly prepared 3:1 ethanol:acetic acid. The fixative was replaced twice, and the fixed sampled stored at 4°C. Flower buds roughly 0.5 mm in size were isolated from inflorescences and washed twice in water and once in citrate buffer (10 mM trisodium citrate, pH 4.5 with HCl), then incubated in a digestion mix [0.3% (*w*/*v*) Pectolyase Y-23 (MP Biomedicals), 0.3% (*w*/*v*) Driselase (Sigma), 0.3% (*w*/*v*) Cellulase Onozuka R10 (Duchefa), 0.1% sodium azide, in 10 mM citrate buffer] for 2 h at 37°C, washed twice with water and kept on ice. Four to five digested buds were transferred to a clean slide and macerated with a bent dissection needle. Roughly 15 µl of 60% acetic acid was added to the mixture and stirred gently at 45°C on a hotplate for 1 min. Another drop of 15 µl of 60% glacial acetic acid was added again to the mixture and stirred for another 1 min. The slide was then flushed with ice-cold 3:1 fixative first around the droplet and then directly. Slides were left to dry tilted at room temperature, then 10 µl of mounting media with 2 µg/ml DAPI was applied to the slide and a coverslip was added. Chromosomes were imaged with a Zeiss Axio Observer epifluorescence microscope.

Immunolocalizations were performed on cells with preserved three-dimensional structures [36]. For male meiocytes, sepals and petals were removed from 0.35 to 0.45 mm flower buds and collected in buffer A (KCl 80 mM, NaCl 20 mM, Pipes–NaOH 15 mM, EGTA 0.5 mM, EDTA 2 mM, sorbitol 80 mM, DTT 1 mM, spermine 0.15 mM, and spermidine 0.5 mM). For female meiocytes, 0.8–1.2 mm pistils were collected and their stigmata were cut off and collected in buffer A. Male and female samples were fixed by incubation in bufferA + 2% formaldehyde for 30 min under vacuum. Buds or pistils were then washed in buffer A for 10 min and digested at 37° for 1 h (0.3% cellulase, 0.3% pectolyase Y23, 0.3% driselase, and 0.1% sodium azide in citrate buffer). After a wash in buffer A, digested buds or pistils were kept in buffer A on ice. To make the embedding, 5–8 buds or pistils were placed in 6 µl of buffer A on a 18 mm ×18 mm high-precision coverslip, and anthers or pistils were dissected and squashed to extrude meiocytes. A 3 µl drop of activated polyacrylamide solution [25 µl 15% polyacrylamide (SIGMA A3574) in buffer A + 1.25 µl of 20% sodium sulfite + 1.25 µl of 20% ammonium persulfate] is added to the meiocytes and a second coverslip is placed on the top, with gentle pressure. The polyacrylamide gels were left to polymerize for 1 h, and then the two coverslips were separated. The coverslips cov-

ered by a gel pad were incubated in 1× PBS, 1% Triton X-100, and 1 mM EDTA for 1 h with agitation, followed by 2 h in blocking buffer (3% BSA in 1× PBS + 0.1% Tween 20) at room temperature. Coverslips were then incubated with 100 µl of primary antibody in blocking buffer at 4°C in a humid chamber for 48 h. Coverslips were washed four times 30 min with 1× PBS, 0.1% Triton X-100. One hundred microliters of the appropriate fluorophore-conjugated secondary antibodies in blocking buffer were applied (1:250) and incubated at room temperature overnight in the dark. Gels were washed four times 20 min with 1× PBS, 0.1% Triton X-100. Six microlitre of SlowFade™ Gold (for super resolution microscopy) + 10 µM DAPI were used for mounting the coverslip with a slide, that was sealed with nail polish. The primary antibodies used were: anti-REC8 raised in rat [37] (lab code PAK036, dilution 1:250), anti-MLH1 raised in rabbit [27] (PAK017, 1:200), and anti-HEI10 raised in chicken [30] (PAK046, 1:5000). Secondary antibodies were Abberior StarRed, StarOrange, and STARgreen for Stimulated emission depletion (STED) microscopy. Images for MLH1/HEI10 co-foci analysis were taken with the Abberior instrument facility line (www.abberior-instruments.com) using 561 and 640 nm excitation lasers (for STAR Orange and STAR Red, respectively) and a 775 nm STED depletion laser. Confocal images were taken with the same instrument with a 485 nm excitation laser (for Stargreen). Images were deconvolved with Huygens Essential version 20.04 (Scientific Volume Imaging, The Netherlands, http://svi.nl), using the Classic Maximum Likelihood Estimation (CMLE) algorithm, with lateral drift stabilization; SNR: 7 for STED images, 20 for confocal images; 40 iterations; and quality threshold: 0.5. Maximum intensity projections and contrast adjustments were done with Huygens Essential. The Spots tool in Imaris 9.6.1 was used to identify and count HEI10 and MLH1 foci.

Genetic crossover and aneuploidy analysis by sequencing

BC1 populations to be sequenced were grown in the greenhouse for 3 weeks (16 h day/8 h night) and 4 days in the dark. Leaf samples (100–150 mg) were used for DNA extraction and library preparation for Illumina sequencing [38] at the Max Planck Genome Center, Cologne, Germany (https://mpgc.mpipz.mpg.de/home/). To create a list of high-quality single nucleotide poymorphism (SNP) markers, a strategy of combining the whole-genome alignment short-read mapping was used. The raw sequencing data were aligned to the TAIR10 Col reference genome [39] by BWA v0.7.17-r1188 [40] with the default parameters. COs were detected using a sliding window-based method, with a window size of 50 kb and a sliding step of 25 kb [29, 41, 42]. The identified COs were also manually and randomly checked by using inGAP-family [43].

The number of detected COs per plant and their position along the genome are shown in Supplementary Tables S1 and S2. Sequenced samples were individual plants (BC1s) obtained following reciprocal crosses of Col/Ler hybrids of different genotypes (wild type, *mlh1*, *HEI10*±) with wild-type Col plants. For *mlh1*, 159 female BC1 plants (result of [Col/Ler *mlh1*−/−] crossed as female to [wild-type Col] as male) and 124 male BC1 plants (result of the reciprocal cross, [Col/Ler *mlh1*−/−] crossed as male to [wild-type Col] as female) were analyzed. For *HEI10*± 157 female BC1 plants (result of [Col/Ler *HEI10*±] crossed as female to wild-type Col as male) and 126 male BC1 plants (result of the reciprocal cross) were analyzed. For wild-type controls, we used (i) Col/Ler wild-type (*MLH1* +/+) sister plants of the *mlh1*−/− reciprocally crossed with Col (47 female BC1 and 47 male BC1), (ii) and Col/Ler wild-type (HEI10+/+) sister plants of HEI10±, reciprocally crossed with Col (47 female BC1 and 47 male BC1). In addition, for CO distribution and CO interference, we used (iii) wild-type female and male populations from two previous studies: 428 female BC1 and 294 male BC1 plants, ArrayExpress number E-MTAB-11254 [41] and 47 female BC1 and 48 male BC1 plants, ArrayExpress number E-MTAB-12838 [44]. There is no significant difference in the frequency of crossover detected in the different wild-type populations (Supplementary Fig. S2).

To analyze CO interference, we calculated the coefficient of coincidence (CoC) using the MADpattern algorithm as described in [45] with a number of nine intervals (same number of intervals for each chromosome). L_int values were calculated as described in [46]. Both can be conveniently calculated using the online tool https://zwicker-group.github.io/crossover-interference-length/measure_CO_interference.html. The sequencing depths of each chromosome were evaluated by Mosdepth v0.2.7 [29, 47], with a window size of 100 kb. Samples with more than a 1.2-fold difference in sequencing depths between two chromosomes were considered aneuploid.

Results and discussion

MLH1 and MLH3 are partially dispensable for class I CO formation

The *zmm* mutants in *Arabidopsismsh4*, *msh5*, *shoc1*, *ptd1*, *hei10*, and *zip4* (homologs of the yeast *msh4*, *msh5*, *zip2*, *spo16*, *zip3*, and *zip4*, respectively) exhibit a ∼85% reduction in CO formation leading to the presence on average of ∼3 pairs of univalents (among five chromosome pairs) [30, 48–51] (Fig. 1). The residual crossovers in *zmm* mutants are attributed to the class II pathway, which acts in parallel to the *zmm* pathway. Accordingly, combining *zmm* mutations does not reduce further CO formation [52]. We performed chromosome spreads on male meiocytes of *mlh1*, *mlh3*, and the *zmm* representative *msh5* (Fig. 1 and Supplementary Fig. S3). Compared to *msh5*, and other previously characterized *zmm* mutants, both *mlh1* and *mlh3* mutants have a moderate reduction in meiotic CO formation leading to the formation of only ∼1.5 univalent pairs ($P < 10^{-6}$, Fig. 1E, Supplementary Fig. S3) [28, 52]. With ∼12 COs distributed among five chromosome pairs in male wild-type Col meiocytes [41] and assuming that COs are randomly lost, this would correspond to a ∼50% reduction in CO formation. Combining *mlh1* and *mlh3* mutations did not increase the frequency of univalents ($P = .20$, Fig. 1), suggesting that MLH1 and MLH3 act together to promote CO formation. Consistently, MLH1 and MLH3 form co-foci [28]. Further, MLH1 foci formation depends on MLH3: In wild-type diplotene and diakinesis stages, MLH1 and HEI10 form foci with quasi-absolute colocalization (Fig. 1F, $n = 20$ cells, 11.55 co-foci per cell, 231/233 = 99% of HEI10 foci colocalized with MLH1 foci, and 231/234 = 99% of MLH1 foci colocalized with HEI10 foci). In *mlh3*, in contrast, no MLH1 foci were detected ($n = 22$ diplotene and diakine-

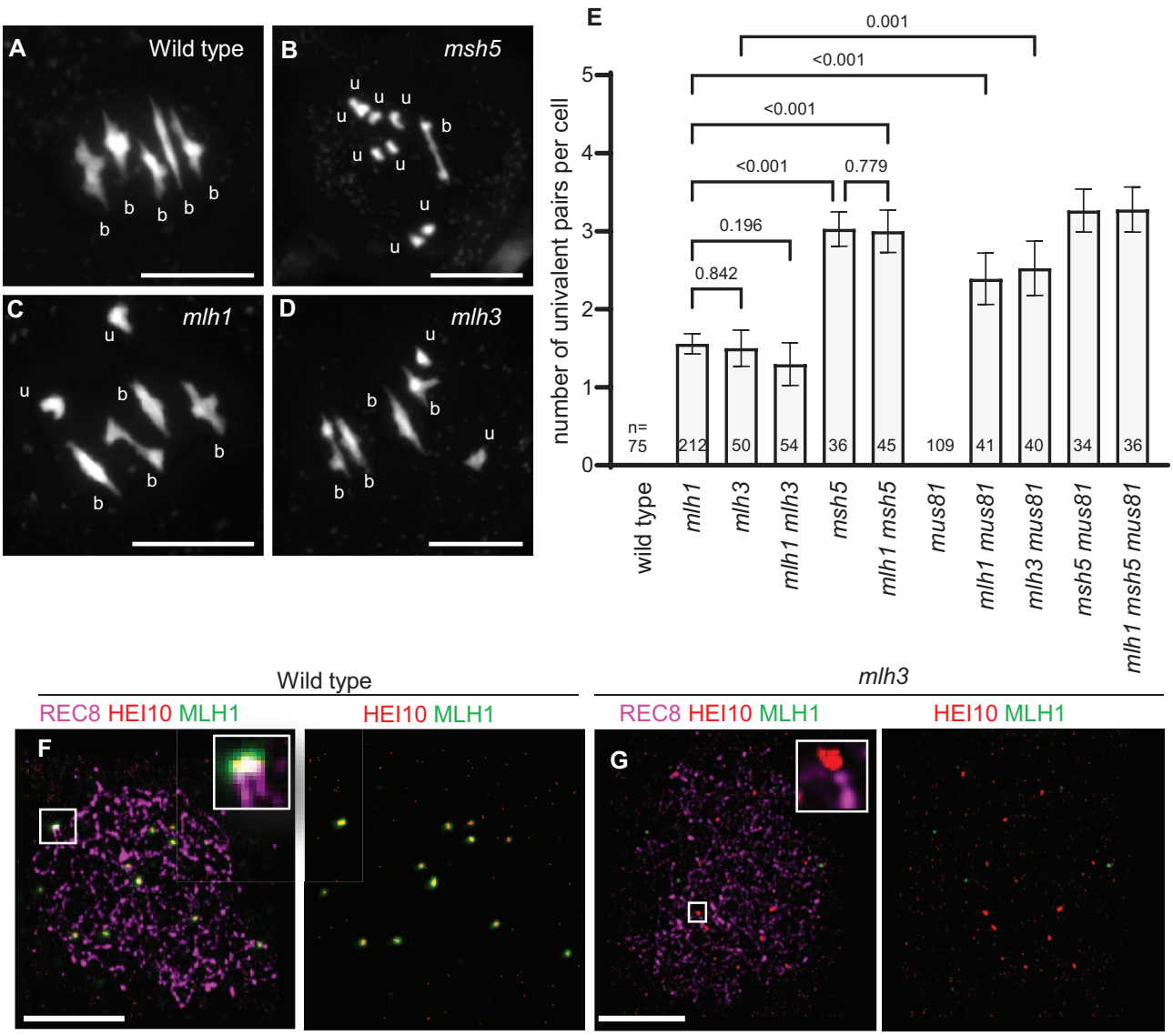

Figure 1. MLH1 and MLH3 are partially dispensable for class I CO formation. (**A**–**D**) Metaphase I chromosome spreads for both wild-type and mutant male meiosis, stained with DAPI. Pairs of homologous chromosomes connected by crossovers are referred to as bivalents, abbreviated as "b." When crossovers are absent and homologous chromosomes are separated, they are referred to as univalents, abbreviated as "u." Scale bar = 10 μm. (**E**) Quantification of the number of univalent pairs per male meiotic cell. If zero pairs of univalents were observed, the bar is not visible. The mean ±95% confidence interval is shown and the number *n* of analyzed cells is indicated. *P* values are Kuskal–Wallis and uncorrected Dunn's test performed in Prism 10.2.0. (F–G) Immunolocalization of REC8 (purple), HEI10 (red), and MLH1 (green) at diakinesis of male meiocytes. Signal shift due to chromatic aberration was corrected using the Chromatic Aberration Wizard of the Huygens software. (**F**) In wild type, MLH1 and HEI10 colocalize in foci. (**G**) In *mlh3*, HEI10 foci are present (see also Fig. 3), but MLH1 foci are not detected. Scale bar = 3 μm.

sis cells, Fig. 1G), while HEI10 foci were observed (see also Fig. 3).

The combination of *mlh3* with *msh5* or with *shoc1* results in a *zmm*-like level of univalents [52]. Similarly, the *mlh1 msh5* mutant is indistinguishable from the *msh5* single mutant in terms of univalent frequency ($P = .78$, Fig. 1E) and is more affected than *mlh1* ($P < 10^{-6}$). This shows that residual class I COs are formed in the absence of MLH1 or/and MLH3. Altogether, this demonstrates that *Arabidopsis* MLH1 and MLH3 act together in the class I/ZMM pathway but with a less essential role than the ZMMs for CO formation. This recapitulates what was previously shown in *Saccharomyces cerevisiae* [8], suggesting the conservation of the respective roles of ZMMs and MutLγ in meiotic recombination.

In absence of MLH1 or MLH3, MUS81 becomes crucial for CO resolution

The yeast and mammal MLH1/MLH3 complex resolve dHJs in a biased manner resulting exclusively in COs [5–10, 20]. In the absence of bias, dHJs resolution is predicted to result in 50% of COs and 50% of NCOs. We suggest that in the absence of *Arabidopsis* MLH1/MLH3, dHJs are also resolved in an unbiased manner, leading to the loss of ~50% of class I COs, explaining the moderate CO reduction in *mlh1* and *mlh3* compared to *zmm* mutants. A candidate for supporting this unbiased activity is the structure-specific nuclease MUS81, which is involved in class II CO formation [53]. MUS81 has only a minor role in supporting CO formation, and no univalents are observed in *mus81* mutants

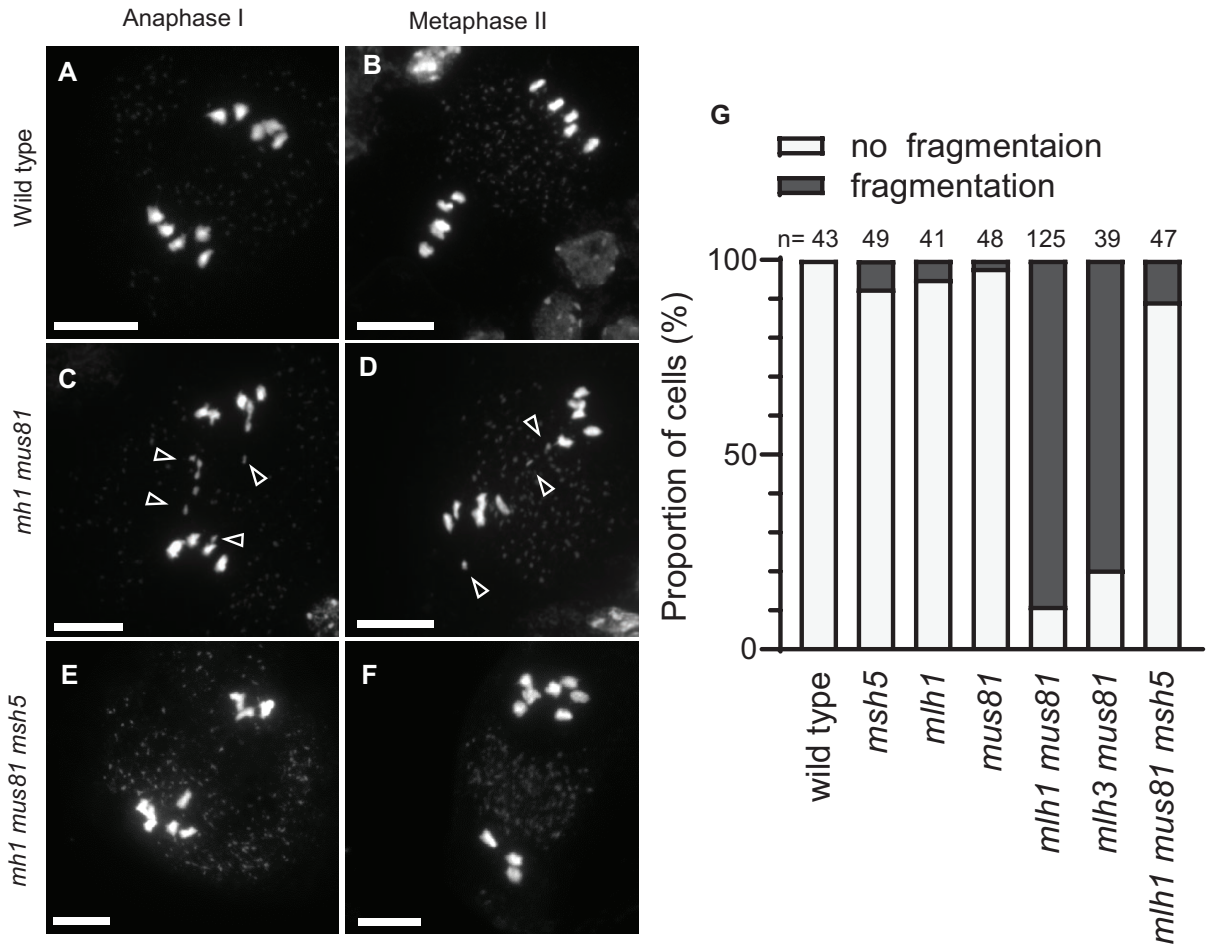

Figure 2. MUS81 becomes crucial for resolving crossovers in the absence of MutLγ. Representative images of anaphase I and metaphase II chromosome spreads from wild type (**A**, **B**) and mutant *mlh1 mus81* (**C**, **D**) and *mlh1 mus81 msh5* (**E**, **F**). Arrowheads indicate chromosome fragments. (**G**) Percentage of cells in which chromosome fragmentation was detected (black) or not (light gray). The numbers above the bar plots indicate the total number of cells analyzed for each genotype. Scale bar = 10 μm.

(Fig. 1E, $n = 109$). Mutating *MUS81* in a *zmm* mutant (*msh4* or *shoc1*) leads to a further reduction of CO formation by ~1/3 but ~0.8 COs per cell are still formed [52, 53], suggesting that other enzymes can compensate for the absence of both ZMMs and MUS81 and contribute to CO formation. This may involve other nucleases such as Yen1 or SLX1/4, as shown in *Saccharomyces cerevisiae* [5]. Mutating *MUS81* in the *mlh1* or *mlh3* background resulted in an increased frequency of univalent pairs from ~1.5 to 2.5, suggesting a substantial decrease in CO formation (Fig. 1E and Supplementary Fig. S3). Furthermore, *mlh1 mus81* and *mlh3 mus81* double mutants showed chromosome fragmentations from anaphase I onward (Fig. 2). This indicates a failure in the resolution of some recombination intermediates when both MLH1/MLH3 and MUS81 are absent. Importantly, chromosome fragmentation in *mlh1 mus81* and *mlh3 mus81* is suppressed by mutating *msh5* (Fig. 2), supporting the conclusion that some recombination intermediates produced by the ZMM pathway (dHJs) fail to be repaired if both MLH1/MLH3 and MUS81 are absent.

MLH1 and MLH3 act downstream of HEI10

In the wild type, the HEI10 protein initially decorates the center of the synaptonemal complex, a large zipper-like structure that associates the homologous chromosomes all along their length [42] and thus appears as a dotted line in between the two homologous axes while they associate (marked by the REC8 Cohesin in Fig. 3A). HEI10 then progressively accumulates in a limited number of large foci that co-localize with MLH1 (Fig. 3B and C). MLH1–HEI10 co-foci mark the sites of COs at the end of pachytene, diplotene, and diakinesis in wild type (Fig. 1F). It is proposed that the dynamic of HEI10—its coarsening—may drive the selection of CO sites [29, 30, 54, 55]. In *mlh1* and *mlh3*, we observed the same initial HEI10 dynamic as in the wild type (Fig. 3D–I): Initially, numerous HEI10 small foci decorate the center of the synaptonemal complex along its entire length (Fig. 3D and G). With meiosis progression, HEI10 gradually forms larger and less numerous foci, culminating in ~12 HEI10 foci at diplotene, indistinguishably in wild type, *mlh1*, and *mlh3* (Fig. 3B, E, H, and J). However, while the number of HEI10 foci is stable from diplotene to diakinesis in the wild type, their number drops dramatically in *mlh1* and *mlh3* (Fig. 3C, F, I, and J). This suggests that MutLγ stabilizes the HEI10 foci in late prophase.

Overexpression of HEI10 ($HEI10^{oe}$), achieved by inserting multiple copies of the *HEI10* gene in wild-type plants (the well-characterized *C2* line) [33], results in an increase in the number of HEI10/MLH1 foci at diplotene and diakinesis,

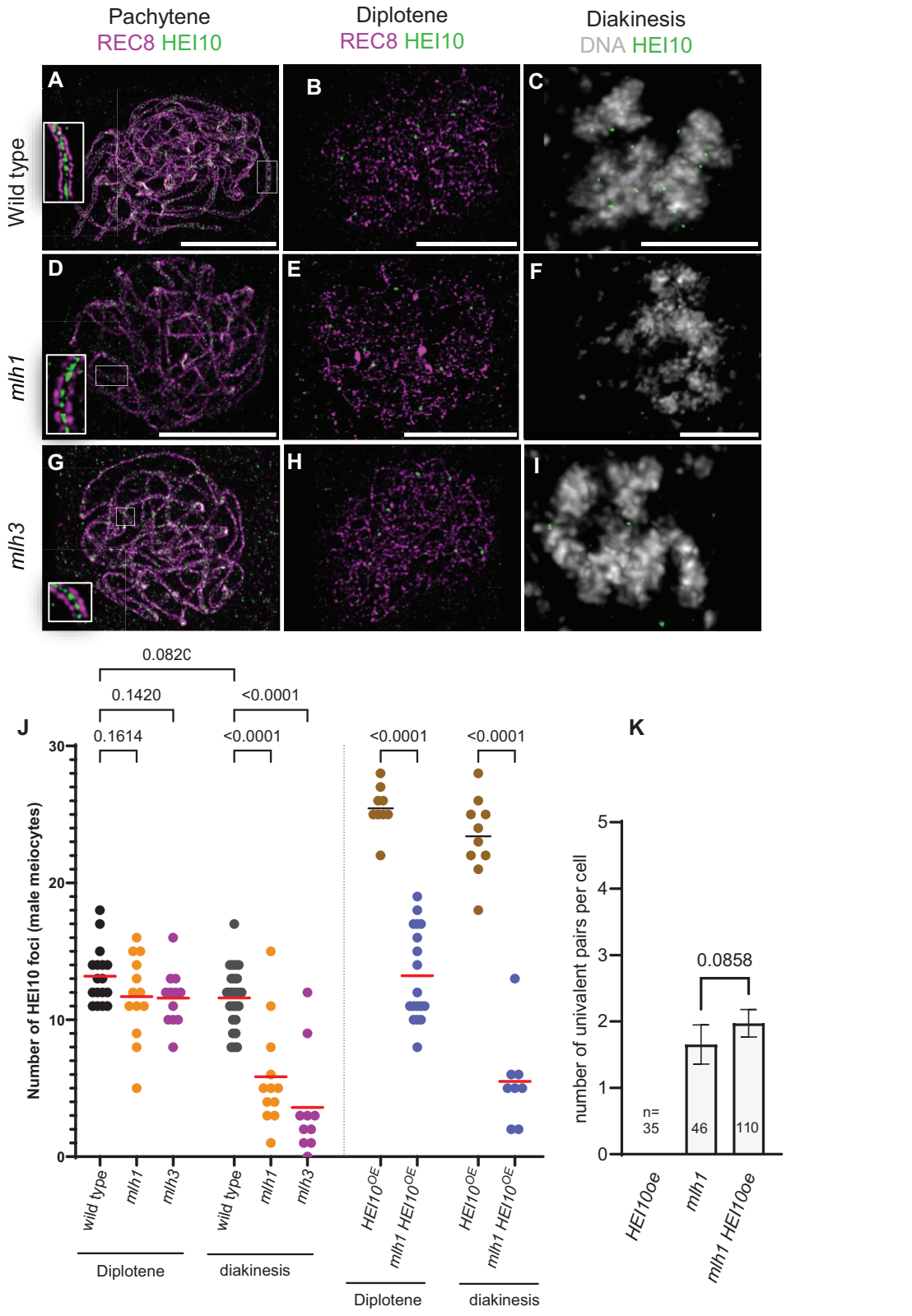

Figure 3. MLH1 and MLH3 stabilize HEI10 foci. (**A**–**I**) Immunostaining of male meiocytes showing REC8 (purple) and HEI10 (green) and DNA (DAPI, gray) from pachytene to diakinesis in wild-type, *mlh1*, and *mlh3* mutants. (**J**) Quantification of HEI10 foci in male meiocytes across genotypes at diplotene and diakinesis stages. Each dot represents a single cell, and the red bar indicates the mean. *P* values are one-way analysis of variance with uncorrected Fisher's least significance difference. (**K**) Number of univalents per male meiotic cell at metaphase I. The mean ±95% confidence interval is shown, and the number *n* of analyzed cells is indicated.

and an increase in CO frequency. [29, 33, 54] (Fig. 3J). Like in wild type (Fig. 1F), the HEI10 foci at diplotene/diakinesis are essentially perfectly colocalized with MLH1 foci ($n = 19$ cells, 463/467 MLH1 foci correspond to HEI10 foci, 467/467 HEI10 foci correspond to MLH1 foci). HEI10 overexpression in *mlh1* also increased the number of HEI10 foci at diplotene, although significantly less than when HEI10 is overexpressed in the wild type, which could reflect the role of MLH1 in the formation and/or the stability of HEI10 foci. However, in *mlh1* HEI10^{oe} diakinesis, the number of foci dropped to a very low level, further supporting the role of MLH1 in stabilizing HEI10 foci (Fig. 3J). We propose that HEI10 accumulates and forms foci at designated CO sites in both wild-type and *mutlγ* mutants, but that in the absence of MutLγ, HEI10 disengages from sites of recombination at late prophase.

Intriguingly, the number of univalents was not reduced in *HEI10^{oe} mlh1* compared to *mlh1* (Fig. 3K and Supplementary Fig. S3), while one could have expected that overexpressing *HEI10* could partially rescue the CO defect in *mlh1*, with more dHJ being stabilized and still 50% of them repaired as CO. This may suggest that the pro-CO activities that resolve dHJ as CO in the absence of MLH1 could be limiting in the context of HEI10 overexpression and outcompeted by dHJ dissolution that does not yield COs.

Genetic crossovers are differently reduced in *mlh1* and *HEI10±*

To explore the effect of *mlh1* on genetic recombination, we generated a novel *mlh1* mutant allele in a second strain (L*er*; *mlh1-3*) using CRISPR (Supplementary Fig. S1) and produced Col/L*er mlh1* hybrids by crossing. The *mlh1-3* Ler mutant had a meiotic defect similar but milder compared to the *mlh1-2* Col, with an average of 0.5 versus 1.4 pairs of univalents at metaphase I in male meiosis, the hybrid being intermediate with an average of 1.1 univalent pairs (Fig. 4A and Supplementary Fig. S3). This may suggest that the Ler *mlh1-3* allele is not null, but we were unable to detect MLH1 foci on *mlh1-3* chromosomes (Supplementary Fig. S4). Less univalents would also be expected if there were more COs in wild-type Ler than in Col, but genetic data show the opposite, with fewer COs in Ler [41]. Further, MLH1 foci are less numerous in wild-type Ler than in Col, the hybrid being intermediate [41] (confirmed here, 10 foci in hybrid versus 11.7 in Col, Mann–Whitney test $P = .0003$, Figs 4F and 1F). Alternatively, the class II CO pathway may be more active in Ler than in Col [56], but analysis of a *msh4* mutant in Ler does not support this proposal [57].

As expected given the presence of univalents, the Col/L*er mlh1* hybrids had reduced fertility (Fig. 4B and C). Hybrids *mlh1* were backcrossed as female or male to wild-type Col, and the resulting progenies were sequenced to analyze recombination in both sexes separately, as previously described [29, 41, 42]. In the wild type, the number of COs per transmitted gamete was substantially higher in males than in females (Fig. 4D, 5.0 COs versus 3.3 COs, two-tailed Mann–Whitney test $P < 10^{-6}$), consistent with previous reports [41, 58]. In *mlh1*, the number of transmitted COs was significantly reduced to 3.6 in males ($P < 10^{-6}$) and to 2.6 in female meiosis ($P = .0002$) (Fig. 4D). Heterochiasmy is thus maintained in *mlh1* with ∼40% more COs in male than female meiosis. Note that these measures likely underestimate the CO defects (or overestimate the residual COs), as achiasmatic chromosomes have less chance to be transmitted. We also detected trisomies in both female (15/159, 9.4%) and male (3/124, 2.4%) populations, consistent with chromosome missegregations due to the presence of univalents at meiosis I.

Based on the result described above, we propose that *mlh1* is defective in CO implementation but not in the designation of CO sites. We thought to compare recombination in *mlh1* to a context in which COs are reduced by a modification of the CO designation process. This is the case when HEI10 levels are reduced, leading to a reduction of COs in plants heterozygous for a defective *HEI10* allele [33, 54]. We produced *HEI10±* hybrids with a wild-type functional *HEI10* allele from L*er* and the *hei10-2* mutant allele from Col [30, 33]. In this *HEI10±* Col/L*er* hybrid context, the number of MLH1/HEI10 foci at diplotene was reduced compared to the corresponding wild type in both female and male meiocytes, consistent with a decrease in class I COs (Fig. 4F). In contrast to *mlh1*, the number of univalents in *HEI10±* was very low, fertility was maintained at high levels (Fig. 4A and E), and no aneuploidy was detected in progenies (0/126 and 0/157 for females and males, respectively). This suggests that the obligate CO is maintained in *HEI10±* despite a reduced number of COs. This contrasts with *mlh1*, in which the obligate CO is lost while the number of COs designated site appears to be maintained (HEI10 foci at diplotene, Fig. 3). Hybrids *HEI10±* were then backcrossed as female and male to wild-type Col, and the resulting progenies were sequenced to analyze genetic recombination (Fig. 4D). In females, the mean CO number is not significantly reduced (2.97 compared to 3.27 in wild type, $P = .15$), likely reflecting that the number of COs is close to the minimum ensuring the obligate CO (5 COs per meiocyte = 2.5 COs per gamete). The number of COs in females is slightly lower in *mlh1* than in *HEI10±* ($P = .0049$, Fig. 4D). In *HEI10±* males, the number of COs was significantly reduced compared to the wild type (from 5 to 3.9, $P = 7.10^{-6}$), reaching similar levels than in *mlh1* males ($P = .18$, Fig. 4D). Beyond the reduction in CO numbers, the distribution of CO along chromosomes is not dramatically affected in *mlh1* and *hei10±* compared to wild type (Fig. 5A and Supplementary Fig. S2). In *HEI10±*, only two intervals (2 Mb intervals, chi-square tests with FDR correction) were significantly different from wild type in male meiosis, at terminal intervals of chromosomes 4 and 5 (green stars in Fig. 5A). When comparing *mlh1* to the wild type, two intervals were also significantly different in male meiosis, in distal positions of long chromosome arms (orange stars in Fig. 5A), where CO frequencies are high in male wild-type meiosis. It should be noted again that these genetic data are unavoidably based on the surviving gametes and thus underestimate the decrease in CO frequencies.

CO interference prevents the occurrence of close double-COs. It can be analyzed with the coefficient of coincidence (CoC), which divides the observed frequency of COs occurring concomitantly in two intervals by the expected frequency if COs were independent (product of the frequencies of COs in each interval). For example, if two intervals have each a frequency of CO of 0.1 (10% of the gametes received a CO in that interval), under the hypothesis of independence of CO events (no interference), one would expect 1% (0.1 × 0.1) of the gametes to have one CO in both intervals simultaneously (double-COs). The observation of a lower frequency of double-COs (e.g. 0.2%) would indicate CO interference and is measured by a CoC value of 0.2 (0.2%/1%). A CoC of

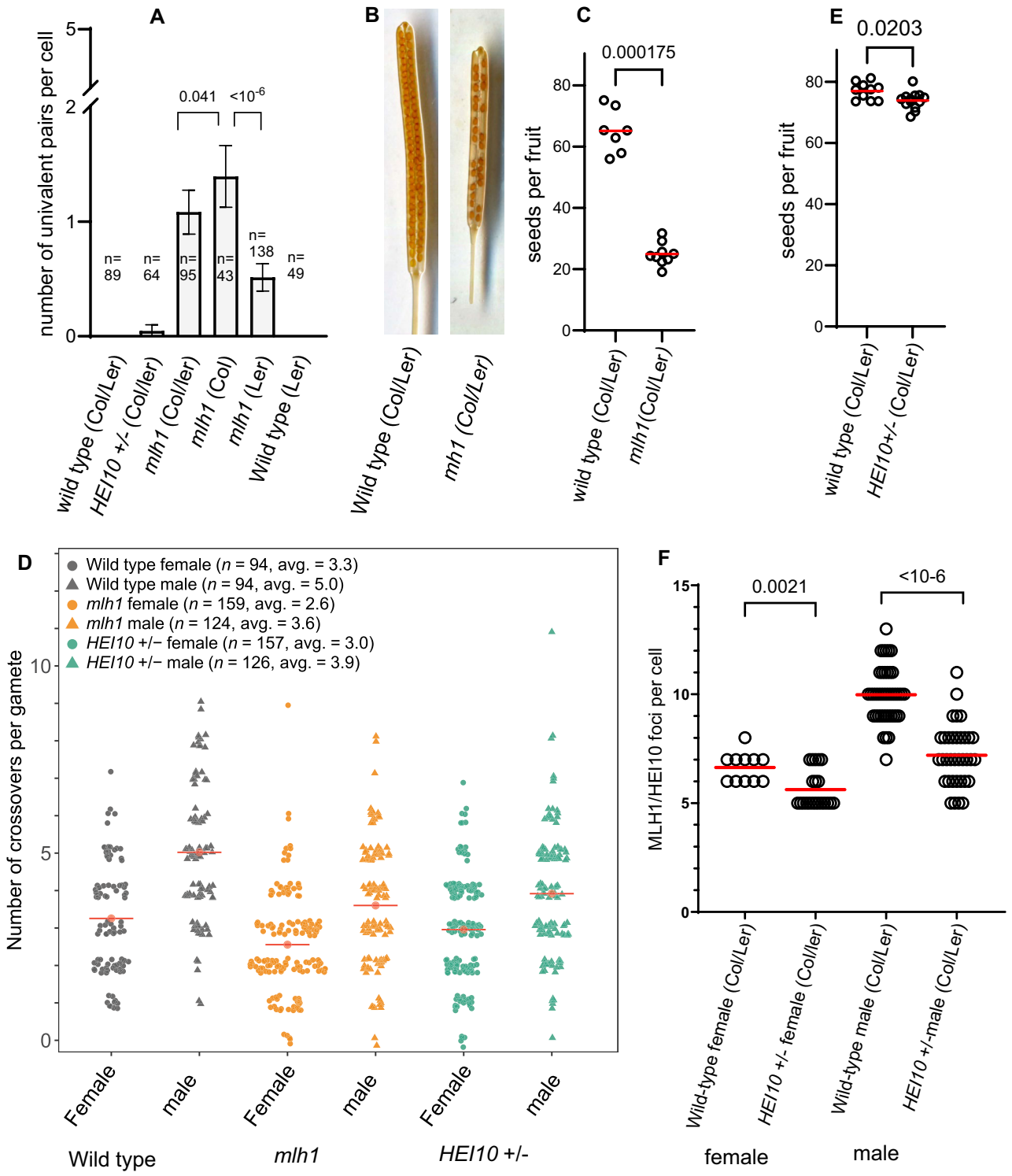

Figure 4. Genetic crossovers are differently affected in *mlh1* and *HEI10*±. (**A**) Quantifying of the number of univalent pairs at metaphase I of male meiosis in Col/L*er* F1 hybrids of three different genotypes (wild-type *mlh1-/-* and *HEI10*±). If no univalent pairs are observed, no bars are displayed. The number *n* of analyzed cells is indicated. Bars indicate mean ± SEM. (**B**) Representative images of fruits from wild-type and *mlh1* mutant hybrid plants. (**C**) Quantification of fertility in *mlh1* hybrids. Each dot represents the average number of seeds per fruit (out of 10 fruits) for an individual plant. The red line indicates the mean number of seeds per fruit for a given genotype. *P* values are Mann–Whitney tests. (**D**) Number of genetic crossovers per transmitted gamete in back-cross populations (Sina plot). Each dot corresponds to an individual female (circle) and male (triangle) gamete. Red lines indicate the mean CO number. The number of analyzed gametes and the average crossover genotype for each sex/genotype are shown. (**E**) Quantification of fertility in *HEI10*± hybrids. Each dot represents the average number of seeds per fruit (out of 10 fruits) for an individual plant. The red line indicates the mean number of seeds per fruit for a given genotype. Statistical significance was assessed using the Mann–Whitney test. (**F**) Quantification of HEI10/MLH1 co-foci in *HEI10*± male meiocytes at diplotene and diakinesis stage. Each dot represents a cell, and the horizontal red bar indicates the mean. *P* values are Mann–Whitney test.

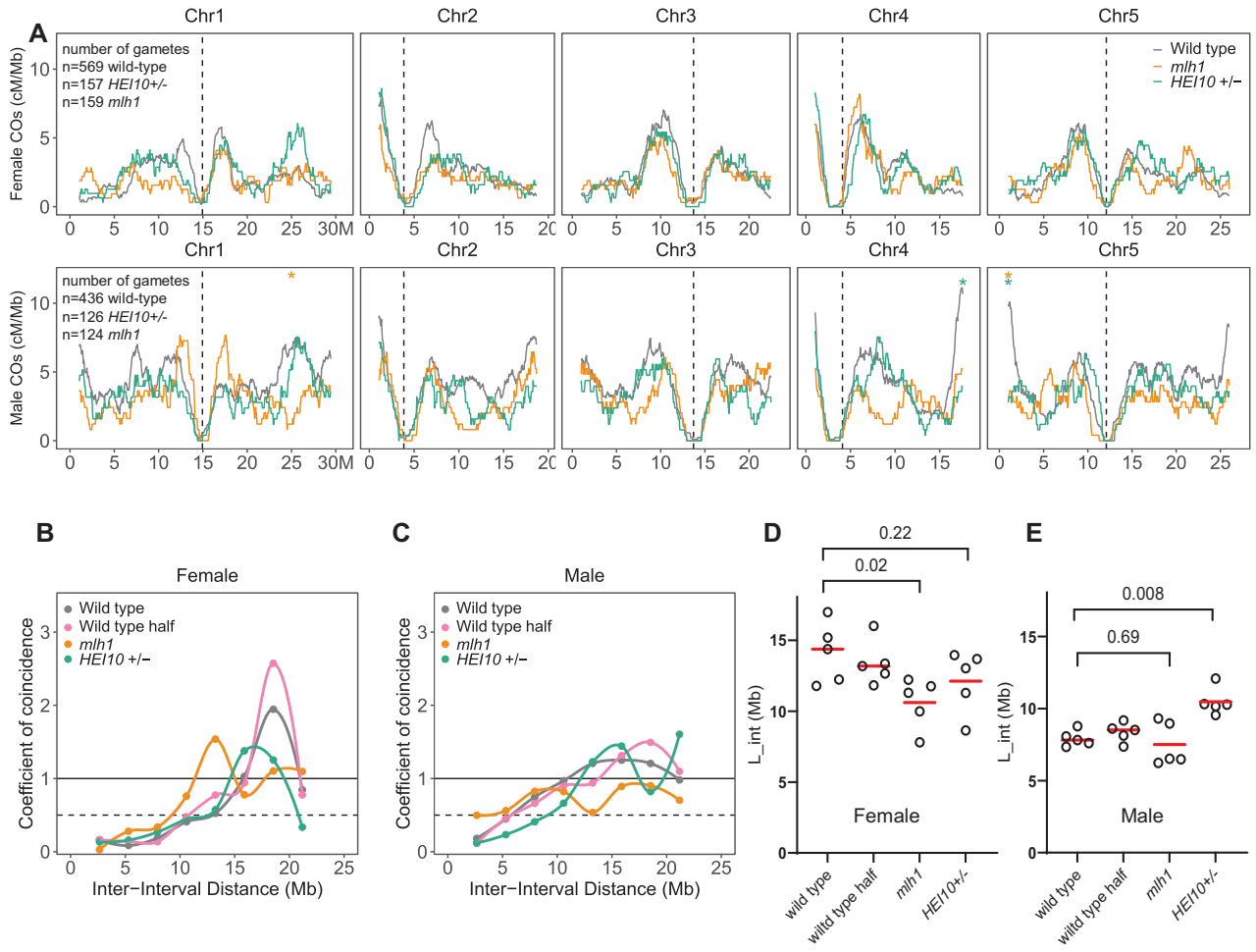

Figure 5. Crossover distribution and interference in *mlh1* and *HEI10*±. (**A**) Distribution of crossovers along chromosomes in females (top) and males (bottom) of wild type, *mlh1*, and *HEI10*±. A window size of 2 Mb with a step size of 50 kb was used for plotting. The Y axis is CO frequency in centimorgan per Mb. The X-axis is the position in Mb (TAIR10). The vertical dashed line marks the position of the centromere. To gain power wild-type data from previous experiments were pooled with wild types from this study (Supplementary Fig. S2). The number of analyzed samples *n* (BC1 plants, or transmitted gamete) are indicated for each genotype. Intervals (2 Mb) that are significantly different between wild type and mutants are indicated by stars (chi-square with FDR correction for multiple testing). (**B**) CoC curves for female and male meiosis. The CoC is displayed on the Y-axis, while the X-axis shows the inter-interval distance in Mb. A CoC value of one suggests independent CO occurrence, whereas a value near zero indicates crossover interference. The analyzed samples are the same as in panel (A). (**D**, **E**) Interference length (L_int), which measures the shift in inter-CO distances due to interference. Higher L_int values indicate stronger crossover interference. Each dot is the L-int for an individual chromosome. Tests are two-tailed Mann–Whitney test.

one indicates that COs occur independently of one another, while a CoC close to zero reveals strong CO interference. A CoC curve is obtained by dividing chromosomes into a certain number of intervals (nine in the present study), considering all the possible pairs of intervals, and plotting the CoC values versus the distances separating the pairs of considered intervals [45, 55]. For example, the first point (shortest distance) of the curve corresponds the CoC value when considering all the pairs of adjacent intervals. Note that CoC values tend to be noisy for the largest distances (because along a chromosome, there are fewer pairs of distant intervals than pairs of adjacent intervals). In wild type, CoC curves are below 1 for short inter-interval distances in both female and male meiosis, confirming the presence of CO interference (Fig. 5B and C). When measured in the genomic space, interference is stronger in wild-type female meiosis, with the CoC curve reaching 1 at ~16 Mb, compared to males where the curve reaches 1 at shorter distances (~11 Mb).

Another newly developed method to measure interference is L_int, which computes the shift in inter-CO distances due to interference [46]. One key innovation of L_int is that it considers distances between all pairs of COs on a chromosome and not only adjacent COs (see details of the development of the method in [46]). One advantage of L_int is that it provides a numerical value of interference (0 indicating the absence of CO interference) that we computed for each chromosome. In the wild type, L_int values are larger in female than male datasets, confirming the strongest CO interference in the genomic space (Fig. 5D and E). This is consistent with previous observations and is attributed to shorter (μm) chromosome axis in females (with the same amount of DNA), leading to stronger interference in the genomic space [29, 41, 42, 58].

One intrinsic mathematical property of CO interference as measured by these two methods is the insensitivity to random sub-sampling of CO. Theoretically and by construction, losing randomly half of the COs maintains identical CoC curves and L_int values [46, 59]. To illustrate this property, we randomly eliminated half of the COs in the wild-type dataset, and as expected, the CoC curves and L_int were not significantly modified (Fig. 5B–E).

In *HEI10*± males, interference was increased in comparison to wild type, with the CoC curve shifted to the right and increased L_int values (Fig. 5C and E). This is consistent with previous cytological observations, which concluded that decreased HEI10 levels increase interference and concomitantly reduce CO numbers, as predicted by the coarsening model [54]. This supports the hypothesis that in *HEI10*± males, the decrease in COs is due to a modified process of CO designation. In *HEI10*± females, the CoC curve and L_int were not significantly modified (Fig. 5B and D), consistent with a nonsignificant decrease in CO number (Fig. 4D), probably because interference is already very strong in wild-type females.

In *mlh1*, even if CO numbers are strongly reduced (more than in *HEI10*±), the CO interference was not increased. In males, the CoC value for the adjacent intervals may indicate decreased interference, but this is not supported by the rest of the CoC curve, nor by the L_int values, which are not reduced ($P = .7$). This is in clear contrast to *HEI10*± males, where reduced CO number is associated with increased interference. In females, the CoC values are slightly higher for *mlh1* than for the wild type, and L_int values are significantly reduced (from 14.1 to 10.6, $P = .016$), both indicating a slight decrease in CO interference. This suggests that the CO defect in MLH1 is not associated with a modification of the designation process (i.e. increase in interference), and is consistent with the proposal that implementation is defective, with a fraction of the designated site randomly failing to produce COs, reducing CO number without or with a minor effect on interference values.

Altogether, we suggest that the function of MLH1/MLH3 in *Arabidopsis* is to impose designated recombination intermediates to be resolved exclusively as COs, a role similar to that in yeast and mammals [10, 20, 21]. This proposal is notably based on: (i) Mutating *MLH1*, *MLH3*, or both leads to a moderate reduction of COs in *mlh1* or *mlh3*, compared to *zmm* mutants. The obligate CO is lost, and the frequency of univalents suggests a ∼50% reduction in COs. A similar observation was made in rice, suggesting a conserved role in the flowering plant clade [60, 61]. (ii) Epistasis analyses show that MLH1/3 act late in the classI/ZMM pathway, but with a less prominent role than ZMMs. (iii) CO interference is maintained in *mlh1*. Our data also suggest that in the absence of MLH1/3 in *Arabidopsis*, CO-designated intermediates (dHJs) are repaired by alternative enzymes, such as MUS81, that promote CO formation less efficiently, failing to ensure CO formation. In the absence of both MutLγ and MUS81, CO frequency is reduced, and chromosome fragments are observed at anaphase I, suggesting unrepaired recombination intermediates. These fragments are dependent on *MSH5*, suggesting that they result from unrepaired dHJ. Remarkably similar results and conclusions were previously obtained in *Saccharomyces cerevisiae*, suggesting a conserved function of MutLγ in the ZMM pathway [5–10]. These conclusions are compatible with the proposed role for MLH1/MLH3 in yeast and mammals—asymmetric resolution of dHJs exclusively as CO [17, 18, 20, 21]—and suggest that this function is widely conserved in eukaryotes.

HEI10 and MLH1 form co-foci at recombination sites from late pachytene to diakinesis in wild-type *Arabidopsis*. In *mlh1* and *mlh3* mutants, HEI10 foci are present at diplotene, consistent with MutLγ acting late in the recombination process, downstream of CO designation; however, the number of HEI10 foci drops at diakinesis, suggesting that MutLγ stabilizes HEI10 foci. Several hypotheses can be proposed for how MutLγ might stabilize HEI10 foci. MLH1 and HEI10 form matching co-foci, suggesting that they are mixed in co-condensates from late pachytene onward. MutLγ could contribute to the stability of these condensates, especially during the process of chromosomal compaction that characterizes diakinesis. In this scenario, the absence of MutLγ would lead to the dissolution of HEI10 foci, leaving the recombination intermediates they covered unprotected. Alternatively, MutLγ could directly protect recombination intermediates from competing cleavage activities (e.g. nucleases). In this second scenario, the recombination intermediate would be rapidly resolved, which in turn would lead to the desegregation of HEI10 foci. In mice, MutLγ also regulates the stable accumulation of HEI10 at CO sites [62], but the comparison between these two species not straightforward, with the existence of three interdependent pro-CO RING domain proteins in mice (HEI10, RNF212, and RNF212B) [63, 64], and only one in *Arabidopsis* (HEI10, no homolog of RNF212 in the genome).

In *Saccharomyces cerevisiae*, *S. macrospora*, and mice, several studies pointed to an additional earlier role for MLH1 and/or MLH3 in the meiotic recombination process [9, 10, 65–68]. We cannot exclude an additional earlier role of MLH1 or MLH3 in *Arabidopsis*, but our data do not suggest a role prior to CO resolution. If an earlier role exists, it has no or a minor impact on the number of CO events. Finally, it should be noted that MLH1/MLH3 are not found in some species/lineages such as *Drosophila melanogaster* and *Caenorhabditis elegans*, suggesting they evolved alternative mechanisms to ensure CO maturation.

Acknowledgements

We thank Ian Henderson for kindly providing the HEI10oe C2 line.

Author contributions: S.D., Q.L., V.S., and J.B.F. produced data. S.D., Q.L., V.S., J.B.F., and R.M. analyzed data. S.D., Q.L., and R.M. prepared the figures. S.D., Q.L., J.B.F., and R.M. wrote and edited the manuscript. R.M. conceptualized the project.

Supplementary data

Supplementary data is available at NAR online.

Conflict of interest

None declared.

Funding

This work was supported by core funding from the Max Planck Society, and Alexander von Humboldt Fellowships to Q.L. and J.B.F. Funding to pay the Open Access publication charges for this article was provided by Max Planck Gesellschaft.

Data availability

The number and list of identified COs in the female and male populations of wild type, *mlh1*, and *hei10*± can be accessed in Supplementary Tables S1 and S2. The raw sequencing data generated in this study have been deposited in the ArrayExpress EMBL-EBI database under accession codes E-MTAB-14422 and E-MTAB-14423.

This paper is linked to: doi:10.1093/nar/gkaf187.

References

1. Hunter N. Meiotic recombination: the essence of heredity. *Cold Spring Harb Perspect Biol* 2015;**7**:a016618. https://doi.org/10.1101/cshperspect.a016618
2. Szostak JW, Orr-Weaver TL, Rothstein RJ *et al.* The double-strand-break repair model for recombination. *Cell* 1983;**33**:25–35. https://doi.org/10.1016/0092-8674(83)90331-8
3. Schwacha a, Kleckner N. Identification of double Holliday junctions as intermediates in meiotic recombination. *Cell* 1995;**83**:783–91. https://doi.org/10.1016/0092-8674(95)90191-4
4. Börner GV, Kleckner N, Hunter N. Crossover/noncrossover differentiation, synaptonemal complex formation, and regulatory surveillance at the leptotene/zygotene transition of meiosis. *Cell* 2004;**117**:29–45. https://doi.org/10.1016/S0092-8674(04)00292-2
5. Zakharyevich K, Tang S, Ma Y *et al.* Delineation of joint molecule resolution pathways in meiosis identifies a crossover-specific resolvase. *Cell* 2012;**149**:334–47. https://doi.org/10.1016/j.cell.2012.03.023
6. Allers T, Lichten M. Differential timing and control of noncrossover and crossover recombination during meiosis. *Cell* 2001;**106**:47–57. https://doi.org/10.1016/S0092-8674(01)00416-0
7. Argueso JL, Kijas AW, Sarin S *et al.* Systematic mutagenesis of the *Saccharomyces cerevisiae* MLH1 gene reveals distinct roles for Mlh1p in meiotic crossing over and in vegetative and meiotic mismatch repair. *Society* 2003;**23**:873–86.
8. Argueso JL, Wanat J, Gemici Z *et al.* Competing crossover pathways act during meiosis in *Saccharomyces cerevisiae*. *Genetics* 2004;**168**:1805–16. https://doi.org/10.1534/genetics.104.032912
9. Marsolier-Kergoat M-CC, Khan MM, Schott J *et al.* Mechanistic view and genetic control of DNA recombination during meiosis. *Mol Cell* 2018;**70**:9–20. https://doi.org/10.1016/j.molcel.2018.02.032
10. Sanchez A, Adam C, Rauh F *et al.* Exo1 recruits Cdc5 polo kinase to MutLγ to ensure efficient meiotic crossover formation. *Proc Natl Acad Sci USA* 2020;30577–88. https://doi.org/10.1073/pnas.2013012117
11. Lipkin SM, Moens PB, Wang V *et al.* Meiotic arrest and aneuploidy in MLH3-deficient mice. *Nat Genet* 2002;**31**:385–90. https://doi.org/10.1038/ng931
12. Edelmann W, Cohen PE, Kane M *et al.* Meiotic pachytene arrest in MLH1-deficient mice. *Cell* 1996;**85**:1125–34. https://doi.org/10.1016/S0092-8674(00)81312-4
13. Hunter N, Borts RH. Mlh1 is unique among mismatch repair proteins in its ability to promote crossing-over during meiosis. *Genes Dev* 1997;**11**:1573–82.
14. Wang TF, Kleckner N, Hunter N. Functional specificity of MutL homologs in yeast: evidence for three Mlh1-based heterocomplexes with distinct roles during meiosis in recombination and mismatch correction. *Proc Natl Acad Sci USA* 1999;**96**:13914–9. https://doi.org/10.1073/pnas.96.24.13914
15. Nishant KT, Plys AJ, Alani E. A mutation in the putative MLH3 endonuclease domain confers a defect in both mismatch repair and meiosis in *Saccharomyces cerevisiae*. *Genetics* 2008;**179**:747–55. https://doi.org/10.1534/genetics.108.086645
16. Ranjha L, Anand R, Cejka P. The *Saccharomyces cerevisiae* Mlh1–Mlh3 heterodimer is an endonuclease that preferentially binds to Holliday junctions. *J Biol Chem* 2014;**289**:5674–86. https://doi.org/10.1074/jbc.M113.533810
17. Rogacheva MV, Manhart CM, Chen G *et al.* Mlh1–Mlh3, a meiotic crossover and DNA mismatch repair factor,is a Msh2–Msh3-stimulated endonuclease. *J Biol Chem* 2014;**289**:5664–73. https://doi.org/10.1074/jbc.M113.534644
18. Manhart CM, Ni X, White MA *et al.* The mismatch repair and meiotic recombination endonuclease Mlh1–Mlh3 is activated by polymer formation and can cleave DNA substrates in trans. *PLoS Biol* 2017;**15**:e2001164. https://doi.org/10.1371/journal.pbio.2001164
19. Manhart CM, Alani E. Roles for mismatch repair family proteins in promoting meiotic crossing over. *DNA Repair (Amst)* 2016;**38**:84–93. https://doi.org/10.1016/j.dnarep.2015.11.024
20. Kulkarni DS, Owens SN, Honda M *et al.* PCNA activates the MutLγ endonuclease to promote meiotic crossing over. *Nature* 2020;**586**:623–7. https://doi.org/10.1038/s41586-020-2645-6
21. Cannavo E, Sanchez A, Anand R *et al.* Regulation of the MLH1–MLH3 endonuclease in meiosis. *Nature* 2020;**586**:618–22. https://doi.org/10.1038/s41586-020-2592-2
22. Baker SM, Plug AW, Prolla TA *et al.* Involvement of mouse Mlh1 in DNA mismatch repair and meiotic crossing over. *Nat Genet* 1996;**13**:336–42. https://doi.org/10.1038/ng0796-336
23. Anderson LK, Reeves A, Webb LM *et al.* Distribution of crossing over on mouse synaptonemal complexes using immunofluorescent localization of MLH1 protein. *Genetics* 1999;**151**:1569–79. https://doi.org/10.1093/genetics/151.4.1569
24. Hollingsworth NM, Brill SJ. The Mus81 solution to resolution: generating meiotic crossovers without Holliday junctions. *Genes Dev* 2004;**18**:117–25.
25. Wang Y, Copenhaver GP. Meiotic recombination: mixing it up in plants. *Annu Rev Plant Biol* 2018;**69**:577–609. https://doi.org/10.1146/annurev-arplant-042817-040431
26. Mercier R, Mezard C, Jenczewski E *et al.* The molecular biology of meiosis in plants. *Annu Rev Plant Biol* 2015;**66**:297–327. https://doi.org/10.1146/annurev-arplant-050213-035923
27. Chelysheva L, Grandont L, Vrielynck N *et al.* An easy protocol for studying chromatin and recombination protein dynamics during *Arabidopsis thaliana* meiosis: immunodetection of cohesins, histones and MLH1. *Cytogenet Genome Res* 2010;**129**:143–53. https://doi.org/10.1159/000314096
28. Jackson N, Sanchez-Moran E, Buckling E *et al.* Reduced meiotic crossovers and delayed prophase I progression in AtMLH3-deficient *Arabidopsis*. *EMBO J* 2006;**25**:1315–23. https://doi.org/10.1038/sj.emboj.7600992
29. Durand S, Lian Q, Jing J *et al.* Joint control of meiotic crossover patterning by the synaptonemal complex and HEI10 dosage. *Nat Commun* 2022;**13**:5999. https://doi.org/10.1038/s41467-022-33472-w
30. Chelysheva L, Vezon D, Chambon A *et al.* The *Arabidopsis* HEI10 is a new ZMM protein related to Zip3. *PLoS Genet* 2012;**8**:e1002799. https://doi.org/10.1371/journal.pgen.1002799
31. Dion E, Li L, Jean M *et al.* An *Arabidopsis* MLH1 mutant exhibits reproductive defects and reveals a dual role for this gene in mitotic recombination. *Plant J* 2007;**51**:431–40. https://doi.org/10.1111/j.1365-313X.2007.03145.x
32. Hartung F, Suer S, Bergmann T *et al.* The role of AtMUS81 in DNA repair and its genetic interaction with the helicase

AtRecQ4A. *Nucleic Acids Res* 2006;**34**:4438–48. https://doi.org/10.1093/nar/gkl576
33. Ziolkowski Pa, Underwood CJ, Lambing C *et al.* Natural variation and dosage of the HEI10 meiotic E3 ligase control *Arabidopsis* crossover recombination. *Genes Dev* 2017;**31**:306–17. https://doi.org/10.1101/gad.295501.116
34. Grutzner R, Martin P, Horn C *et al.* High-efficiency genome editing in plants mediated by a Cas9 gene containing multiple introns. *Plant Commun* 2021;**2**:100135. https://doi.org/10.1016/j.xplc.2020.100135
35. Ross KJ, Fransz P, Armstrong SJ *et al.* Cytological characterization of four meiotic mutants of *Arabidopsis* isolated from T-DNA-transformed lines. *Chromosome Res* 1997;**5**:551–9. https://doi.org/10.1023/A:1018497804129
36. Hurel A, Phillips D, Vrielynck N *et al.* A cytological approach to studying meiotic recombination and chromosome dynamics in *Arabidopsis thaliana* male meiocytes in three dimensions. *Plant J* 2018;**95**:385–96. https://doi.org/10.1111/tpj.13942
37. Cromer L, Jolivet S, Horlow C *et al.* Centromeric cohesion is protected twice at meiosis, by SHUGOSHINs at anaphase I and by PATRONUS at interkinesis. *Curr Biol* 2013;**23**:2090–9. https://doi.org/10.1016/j.cub.2013.08.036
38. Rowan BA, Heavens D, Feuerborn TR *et al.* An ultra high-density *Arabidopsis thaliana* crossover map that refines the influences of structural variation and epigenetic features. *Genetics* 2019;**213**:771–87. https://doi.org/10.1534/genetics.119.302406
39. Lamesch P, Berardini TZ, Li D *et al.* The *Arabidopsis* Information Resource (TAIR): improved gene annotation and new tools. *Nucleic Acids Res* 2012;**40**:D1202–10. https://doi.org/10.1093/nar/gkr1090
40. Li H, Durbin R. Fast and accurate short read alignment with Burrows–Wheeler transform. *Bioinformatics* 2009;**25**:1754–60. https://doi.org/10.1093/bioinformatics/btp324
41. Lian Q, Solier V, Walkemeier B *et al.* The megabase-scale crossover landscape is largely independent of sequence divergence. *Nat Commun* 2022;**13**:3828. https://doi.org/10.1038/s41467-022-31509-8
42. Capilla-Perez L, Durand S, Hurel A *et al.* The synaptonemal complex imposes crossover interference and heterochiasmy in *Arabidopsis*. *Proc Natl Acad Sci USA* 2021;**118**:e2023613118. https://doi.org/10.1073/pnas.2023613118
43. Lian Q, Chen Y, Chang F *et al.* inGAP-family: accurate detection of meiotic recombination loci and causal mutations by filtering out artificial variants due to genome complexities. *Genomics Proteomics Bioinformatics* 2022;**20**:524–35. https://doi.org/10.1016/j.gpb.2019.11.014
44. Singh DK, Lian Q, Durand S *et al.* HEIP1 is required for efficient meiotic crossover implementation and is conserved from plants to humans. *Proc Natl Acad Sci USA* 2023;**120**:e2221746120. https://doi.org/10.1073/pnas.2221746120
45. Zhang L, Liang Z, Hutchinson J *et al.* Crossover patterning by the beam-film model: analysis and implications. *PLoS Genet* 2014;**10**:e1004042. https://doi.org/10.1371/journal.pgen.1004042
46. Ernst M, Mercier R, Zwicker D. Interference length reveals regularity of crossover placement across species. *Nat Commun* 2024;**15**:8973. https://doi.org/10.1038/s41467-024-53054-2
47. Pedersen BS, Quinlan AR. Mosdepth: quick coverage calculation for genomes and exomes. *Bioinformatics* 2018;**34**:867–8. https://doi.org/10.1093/bioinformatics/btx699
48. Higgins JD, Armstrong SJ, Franklin FC *et al.* The *Arabidopsis* MutS homolog AtMSH4 functions at an early step in recombination: evidence for two classes of recombination in *Arabidopsis*. *Genes Dev* 2004;**18**:2557–70. https://doi.org/10.1101/gad.317504
49. Higgins JD, Vignard J, Mercier R *et al.* AtMSH5 partners AtMSH4 in the class I meiotic crossover pathway in *Arabidopsis thaliana*, but is not required for synapsis. *Plant J* 2008;**55**:28–39. https://doi.org/10.1111/j.1365-313X.2008.03470.x
50. Macaisne N, Novatchkova M, Peirera L *et al.* SHOC1, an XPF endonuclease-related protein, is essential for the formation of class I meiotic crossovers. *Curr Biol* 2008;**18**:1432–7. https://doi.org/10.1016/j.cub.2008.08.041
51. Chelysheva L, Gendrot G, Vezon D *et al.* Zip4/Spo22 is required for class I CO formation but not for synapsis completion in *Arabidopsis thaliana*. *PLoS Genet* 2007;**3**:e83. https://doi.org/10.1371/journal.pgen.0030083
52. Macaisne N, Vignard J, Mercier R. SHOC1 and PTD form an XPF-ERCC1-like complex that is required for formation of class I crossovers. *J Cell Sci* 2011;**124**:2687–91. https://doi.org/10.1242/jcs.088229
53. Higgins JD, Buckling EF, Franklin FC *et al.* Expression and functional analysis of AtMUS81 in *Arabidopsis* meiosis reveals a role in the second pathway of crossing-over. *Plant J* 2008;**54**:152–62. https://doi.org/10.1111/j.1365-313X.2008.03403.x
54. Morgan C, Fozard JA, Hartley M *et al.* Diffusion-mediated HEI10 coarsening can explain meiotic crossover positioning in *Arabidopsis*. *Nat Commun* 2021;**12**:4674. https://doi.org/10.1038/s41467-021-24827-w
55. Girard C, Zwicker D, Mercier R. The regulation of meiotic crossover distribution: a coarse solution to a century-old mystery? *Biochem Soc Trans* 2023;**51**:1179–90. https://doi.org/10.1042/BST20221329
56. Zhu L, Fernandez-Jimenez N, Szymanska-Lejman M *et al.* Natural variation identifies SNI1, the SMC5/6 component, as a modifier of meiotic crossover in *Arabidopsis*. *Proc Natl Acad Sci USA* 2021;**118**:e2021970118. https://doi.org/10.1073/pnas.2021970118
57. Seguela-Arnaud M, Crismani W, Larcheveque C *et al.* Multiple mechanisms limit meiotic crossovers: TOP3alpha and two BLM homologs antagonize crossovers in parallel to FANCM. *Proc Natl Acad Sci USA* 2015;**112**:4713–8. https://doi.org/10.1073/pnas.1423107112
58. Giraut L, Falque M, Drouaud J *et al.* Genome-wide crossover distribution in *Arabidopsis thaliana* meiosis reveals sex-specific patterns along chromosomes. *PLoS Genet* 2011;**7**:e1002354. https://doi.org/10.1371/journal.pgen.1002354
59. Wang S, Hassold T, Hunt P *et al.* Inefficient crossover maturation underlies elevated aneuploidy in human female meiosis. *Cell* 2017;**168**:977–89. https://doi.org/10.1016/j.cell.2017.02.002
60. Xin X, Li X, Zhu J *et al.* OsMLH1 interacts with OsMLH3 to regulate synapsis and interference-sensitive crossover formation during meiosis in rice. *J Genet Genomics* 2021;**48**:485–96. https://doi.org/10.1016/j.jgg.2021.04.011
61. Mao B, Zheng W, Huang Z *et al.* Rice MutLγ, the MLH1–MLH3 heterodimer, participates in the formation of type I crossovers and regulation of embryo sac fertility. *Plant Biotechnol J* 2021;**19**:1443–55. https://doi.org/10.1111/pbi.13563
62. Qiao H, Prasada Rao HBD, Yang Y *et al.* Antagonistic roles of ubiquitin ligase HEI10 and SUMO ligase RNF212 regulate meiotic recombination. *Nat Genet* 2014;**46**:194–9. https://doi.org/10.1038/ng.2858
63. Ito M, Yun Y, Kulkarni DS *et al.* Distinct and interdependent functions of three RING proteins regulate recombination during mammalian meiosis. *Proc Natl Acad Sci USA* 2025;**122**:194–9. https://doi.org/10.1073/pnas.2412961121
64. Condezo YB, Sainz-Urruela R, Gomez HL *et al.* RNF212B E3 ligase is essential for crossover designation and maturation during male and female meiosis in the mouse. *Proc Natl Acad Sci USA* 2024;**121**:e2320995121. https://doi.org/10.1073/pnas.2320995121
65. Duroc Y, Kumar R, Ranjha L *et al.* Concerted action of the MutLβ heterodimer and Mer3 helicase regulates the global extent of meiotic gene conversion. *eLife* 2017;**6**:e21900. https://doi.org/10.7554/eLife.21900
66. Storlazzi A, Gargano S, Ruprich-Robert G *et al.* Recombination proteins mediate meiotic spatial chromosome organization and

pairing. *Cell* 2010;**141**:94–106. https://doi.org/10.1016/j.cell.2010.02.041
67. Premkumar T, Paniker L, Kang R *et al.* Genetic dissection of crossover mutants defines discrete intermediates in mouse meiosis. *Mol Cell* 2023;**83**:2941–58. https://doi.org/10.1016/j.molcel.2023.07.022
68. Al-Sweel N, Raghavan V, Dutta A *et al.* mlh3 mutations in baker's yeast alter meiotic recombination outcomes by increasing noncrossover events genome-wide. *PLoS Genet* 2017;**13**:e1006974. https://doi.org/10.1371/journal.pgen.1006974

Received: September 23, 2024. **Revised:** February 7, 2025. **Editorial Decision:** February 13, 2025. **Accepted:** March 11, 2025
© The Author(s) 2025. Published by Oxford University Press on behalf of Nucleic Acids Research.
This is an Open Access article distributed under the terms of the Creative Commons Attribution-NonCommercial License (https://creativecommons.org/licenses/by-nc/4.0/), which permits non-commercial re-use, distribution, and reproduction in any medium, provided the original work is properly cited. For commercial re-use, please contact reprints@oup.com for reprints and translation rights for reprints. All other permissions can be obtained through our RightsLink service via the Permissions link on the article page on our site—for further information please contact journals.permissions@oup.com.